Original Article | Open Access

Carbon Footprints

Shi *et al. Carbon Footprints* **2026**, *5*, 59 **DOI:**10.20517/cf.2026.115

Database-driven divergence in carbon footprint estimates for Chinese refined copper supply chains

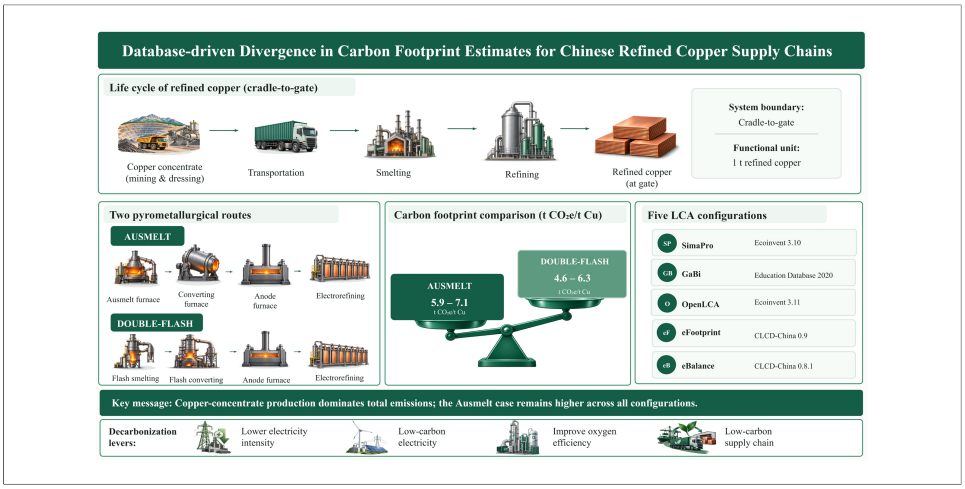
Sihao Shi[1,#], Zhaofeng Zhang[1,#], Qinglin Luo[1], Zhihan Hou[1], Chenjun Hou[2], Wenjuan Dong[3], Tianduo Peng[2,3,4]

Keywords:
Refined copper, carbon footprint, life cycle assessment, multi-configuration comparison

Citation: Shi, S.; Zhang, Z.; Luo, Q.; Hou, Z.; Hou, C.; Dong, W.; Peng, T. Database-driven divergence in carbon footprint estimates for Chinese refined copper supply chains. *Carbon Footprints* **2026**, *5*, 59. https://dx.doi.org/10.20517/cf.2026.115

Received: 2 Aug 2026
First Decision: 21 Aug 2026
Revised: 23 Oct 2026
Accepted: 3 Nov 2026
Published: 12 Nov 2026

Academic Editors:
Liang Dong, Wei-Qiang Chen
Copy Editor:
Ping Zhang
Production Editor:
Ping Zhang



Abstract

Refined copper is critical to the global energy transition, yet carbon footprint estimates for Chinese primary production vary because background databases represent concentrate supply, electricity systems, and process conditions differently. Using 2025 operational data from two Chinese smelters, this study developed cradle-to-gate inventories for Ausmelt-based and double-flash production systems and evaluated them across five software-database-modeling configurations. Across these configurations, the observed Ausmelt case yielded 5.9-7.1 t CO_2e/t Cu, whereas the double-flash case yielded 4.6-6.3 t CO_2e/t Cu. Because feed composition and operating conditions were not normalized, this contrast represents the sampled plant systems rather than an intrinsic technology effect. Upstream concentrate production was the main source of inter-configuration divergence. A controlled parameter-transfer check reproduced the SimaPro result in OpenLCA within 0.008%, indicating transfer fidelity rather than native cross-software equivalence; the estimated OpenLCA-ecoinvent 3.11 result was 1.31% lower than the reconstructed ecoinvent 3.10 case. Paired Monte Carlo analysis confirmed the

Check for updates

[1]Xiuzhong College, Tsinghua University, Beijing 100084, China.
[2]Laboratory of Low Carbon Energy, Tsinghua University, Beijing 100084, China.
[3]Institute of Climate Change and Sustainable Development, Tsinghua University, Beijing 100084, China.
[4]Institute of Carbon Neutrality, Tsinghua University, Beijing 100084, China.
[#]These authors contributed equally.

Correspondence to: Prof. Tianduo Peng, Laboratory of Low Carbon Energy, Tsinghua University, Beijing 100084, China; Institute of Climate Change and Sustainable Development, Tsinghua University, Beijing 100084, China; Institute of Carbon Neutrality, Tsinghua University, Beijing 100084, China. E-mail: ptd@mail.tsinghua.edu.cn

case-level ordering and showed that inter-configuration dispersion exceeded within-configuration parameter uncertainty. After consistently rebasing the electricity-factor trajectory, combined process-efficiency improvement and grid decarbonization reduced modeled electricity-related emissions by approximately 19% in 2030 and 96% in 2060. Oxygen-production efficiency provided additional reductions, although long-term mitigation remained dominated by grid decarbonization. These findings identify low-carbon concentrate supply, efficient air separation, grid decarbonization, and regularly updated localized databases as priorities for comparable refined-copper carbon footprints.

INTRODUCTION

Copper is indispensable to electrification and low-carbon energy systems because of its conductivity, ductility, and extensive use in power networks, transport, buildings, renewable energy, and energy storage[1-6]. Rising demand has increased attention to the environmental burden of copper supply[7-9], and long-term scenario studies project sustained pressure on copper demand and primary supply as low-carbon technologies expand[10-13]. For primary refined copper, emissions occur across mining and beneficiation, concentrate transport, smelting and converting, refining, and the production of energy and auxiliary materials[14,15]; a life-cycle perspective is therefore needed to identify supply-chain hotspots beyond direct plant emissions[16-18].

China is the world's largest producer and consumer of refined copper and a major node in the global copper supply chain[19]. Copper smelting is also an important source of energy use and greenhouse-gas emissions in China's nonferrous-metals sector[20,21]. Cradle-to-gate studies of primary refined copper report about 3.09-9.96 t CO_2e/t Cu [Table 1]. Because national refined-copper output includes secondary production, these primary-production factors are not extrapolated to national aggregate emissions here.

Life cycle assessment (LCA) is widely used to quantify supply-chain environmental burdens[22], but metal-product results are sensitive to foreground inputs, system boundaries, co-product allocation, and background datasets[23]. Comparative LCA studies show that software-database configurations, database coverage, and dataset definitions can materially alter absolute results and, in some cases, decision rankings[24-28]. Refined-copper studies have used inventories based on ecoinvent, Ganzheitliche Bilanzierung (GaBi), and the Chinese Life Cycle Database (CLCD)[29-35]. Sanjuan-Delmás *et al.*[29] reported 4.75 and 3.51 t CO_2e/t Cu for the same Swedish production system using two conventional software-database setups; the present design extends that comparison to five configurations built on a common Chinese plant foreground inventory and adds a controlled cross-platform parameter-transfer check using harmonized ecoinvent 3.10 inventory inputs. Alexander *et al.*[30] compared copper-smelting routes on a concentrate-to-blister boundary, whereas the present study separates cradle-to-gate supply-chain differences from a narrower smelting-and-refining comparison under the plants' observed feed and operating conditions. Plant-based multi-configuration analyses of Chinese primary copper remain limited.

These gaps matter as carbon footprint disclosure, low-carbon procurement, and green-trade requirements expand. A multi-configuration design can reveal which differences are associated with the observed production systems and which are associated with alternative software-database configurations, background datasets, and proxy choices, thereby identifying where harmonization and localization would most improve comparability.

Using operational data from two Chinese primary-copper smelters, this study asks: (1) how the cradle-to-gate footprints and emission profiles of the two observed systems differ under their actual feed and operating conditions; and (2) how strongly alternative software-database-modeling configurations affect the results and

Table 1. Literature on carbon footprint analysis of refined copper

Author(s)	Data year	Study region	System boundary	Functional unit	Allocation approach	Tools and databases	Main findings
Sanjuan-Delmás *et al.*, 2022[29]	2015	Sweden	Cradle-to-gate	1 t 99.99%-pure copper cathode	Economic allocation	SimaPro 9.0 with ecoinvent 3.5; GaBi 9.2	4.75 t CO_2e/t Cu with SimaPro and 3.51 t CO_2e/t Cu with GaBi
Alexander *et al.*, 2021[30]	2020	Global	Copper concentrate to blister copper	1 t copper contained in blister copper	Not reported	HSC Chemistry 9.8, OpenLCA, ecoinvent 3.5	The GWP of blister copper was 434-612 kg CO_2e/t Cu for flash smelting + Peirce-Smith converting (FSF-PSC) and 678-703 kg CO_2e/t Cu for side-blown furnace + top-blown converting (SBF-TBC); electricity (including oxygen production) was the main GWP source and contributed up to 91% for FSF-PSC
Liu *et al.*, 2022[31]	2004-2017	China	Cradle-to-gate	1 t refined copper	Not reported	GaBi with eBalance and yearbooks	Life cycle carbon intensity decreased from 9.96 t CO_2e/t Cu in 2004 to 3.09 t CO_2e/t Cu in 2017; energy consumption and carbon emissions from underground mining were 2.97-7.03 times those from open-pit mining
Lu *et al.*, 2022[32]	2017-2018	China	Cradle-to-gate	1 t standard Cu cathode (i.e., meeting class A in China national standard of GB/T 467-2010)	System expansion by substitution, economic allocation	GaBi with Sphera database	4.28 t CO_2e/t Cu
Chen *et al.*, 2019[33]	2016	China	Cradle-to-gate	1 t refined copper (99.99% cathode copper)	Economic allocation	GaBi and ecoinvent database	3.42 t CO_2e/t Cu for primary copper smelting and 0.316 t CO_2e/t Cu for secondary copper
Song *et al.*, 2014[35]	2009	China	Smelting process	1 t refined copper	Economic allocation	GaBi 4	2,092.26 kg CO_2e/t Cu for flash smelting and 2,203.63 kg CO_2e/t Cu for bath smelting

LCA: Life cycle assessment; GWP: global warming potential; GB/T: recommended national standard of China; HSC: enthalpy, entropy, and heat capacity; GaBi: ganzheitliche bilanzierung.

which processes drive the divergence. A separate smelting-and-refining analysis removes upstream concentrate production and transport without treating the remaining difference as an intrinsic technology effect.

The study contributes plant-based inventories for two major pyrometallurgical systems, a five-configuration comparison using a common foreground inventory, and a controlled parameter-transfer check that evaluates the fidelity of reconstructing a harmonized model in OpenLCA using ecoinvent 3.10 inventory inputs. Allocation sensitivity, paired uncertainty analysis, and electricity-related mitigation scenarios further identify the methodological and operational assumptions that most influence refined-copper carbon footprint estimates.

METHODOLOGY AND DATA

The study applied a cradle-to-gate LCA framework to two observed production systems. For each production route, the same plant-specific foreground inventory was used across five software-database-modeling configurations based on SimaPro, GaBi, OpenLCA, eFootprint, and eBalance [Supplementary Table 1]. Functional unit,

Table 2. Industrial applications and production capacities of the double-flash smelting route in China

Plant	Capacity Year	Capacity (10^4 t/a)
Plant A in Shandong	2007, 2009	40
Plant B in Anhui	2022	48
Plant C in Guangxi	2023	50
Plant D in Fujian	2022, 2023	40
Plant E in Hubei	2023	40

system boundary, and base-case allocation were harmonized across configurations; contribution, sensitivity, uncertainty, and decarbonization analyses were then used to examine result drivers and robustness. Detailed process descriptions and inventories are provided in the Supplementary Materials.

System boundary and functional unit

Primary copper from sulfide concentrates is generally produced through mining and beneficiation, smelting, converting, fire refining, and electrorefining. The two observed systems differ mainly in smelting configuration. Flash smelting reacts dried concentrate rapidly with oxygen-enriched gas in a reaction shaft, whereas Ausmelt uses a submerged lance in an agitated bath and is comparatively tolerant of variable feedstocks[36,37]. Detailed flowsheets are provided in Supplementary Section 1 of the Supplementary Materials.

Smelting off-gas is converted to sulfuric acid, yielding about 3.7 t H_2SO_4/t Cu in the double-flash case and 2.646 t H_2SO_4/t Cu in the Ausmelt case. ISO 14044, issued by the International Organization for Standardization (ISO), prioritizes avoiding allocation where feasible and otherwise requires a justified relationship for partitioning multifunctional-process burdens[38]; harmonization work for metals and the broader allocation literature similarly emphasize physical causality, system expansion, and transparent sensitivity analysis[39-41]. Because sulfuric acid arises from capture and conversion of the SO_2 stream, product mass does not represent the causal relationship governing joint-process burdens. Economic allocation is therefore used as the attributional base case, with zero-value economic allocation, mass allocation, and system expansion evaluated as sensitivity cases.

Using a cathode-copper price of 80,919 Chinese yuan (CNY) per tonne (the rounded arithmetic mean of the 12 monthly national market-monitoring values; see the price-calculation note in Supplementary Section 8.1 of the Supplementary Materials)[42] and the documented 2025 annual-average sulfuric-acid price of 615 CNY/t[43] gives copper allocation fractions of 97.26% for double-flash and 98.03% for Ausmelt. In the sensitivity calculations, the price-derived copper allocation fractions were used without intermediate rounding; the percentages stated above are rounded for reporting. The system-expansion case assumes 1:1 substitution of smelter acid for sulfur-based sulfuric acid with an avoided burden of 0.111 t CO_2e/t H_2SO_4 from ecoinvent 3.11; a zero acid value represents a negligible ex-works-value boundary case.

One plant is evaluated for each production system. Although both technologies are commercially established in China[36,37,44,45], the sampled plants are not treated as statistically representative of all facilities. Representative industrial applications and production capacities of the double-flash route are summarized in Table 2. The primary boundary extends from raw-material acquisition to refined copper at the plant gate. The section titled "Comparison of emissions within a common smelting-and-refining boundary under observed feed and operating conditions" applies a narrower smelting-and-refining boundary covering concentrate pretreatment, smelting, converting, anode-furnace refining, electrorefining, sulfuric-acid production, and oxygen- and nitrogen-production electricity, while excluding upstream concentrate production and transport.

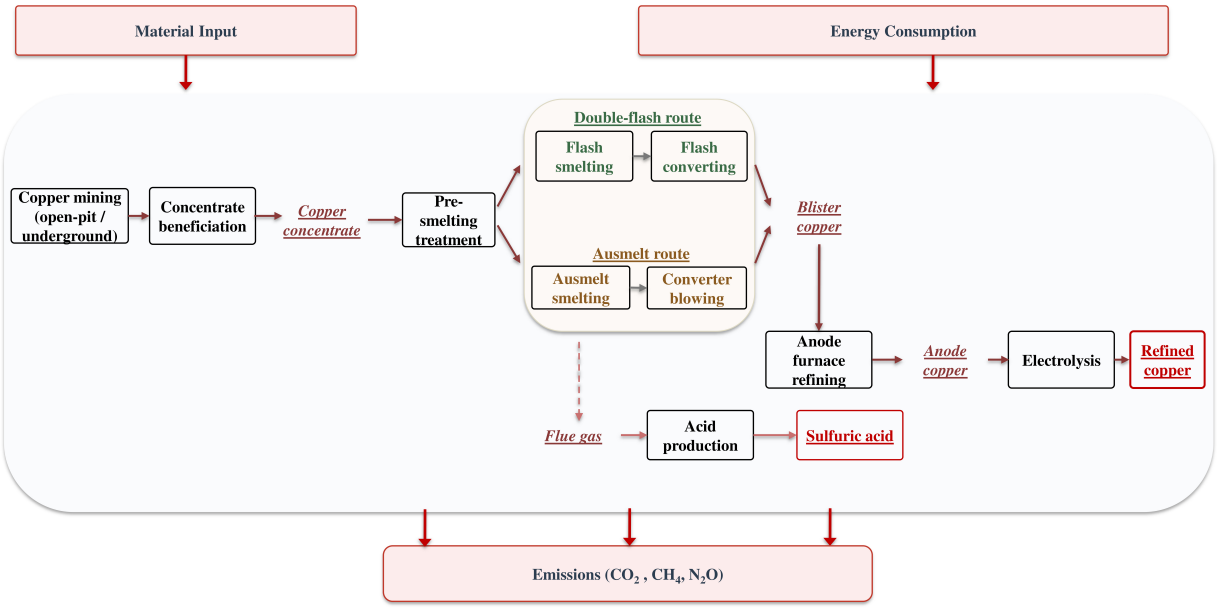


Figure 1. System boundary for the carbon footprint analysis of primary refined copper in China.

The functional unit is 1 t of electrolytically refined copper. Product carbon-footprint quantification is framed consistently with ISO 14067:2018[46]. The inventory includes fossil-energy and relevant process emissions of CO_2, CH_4, and N_2O. Climate impacts are characterized using 100-year global warming potential factors from the Sixth Assessment Report of the Intergovernmental Panel on Climate Change (IPCC)[47] and reported as kg CO_2e/t Cu. The system boundary of the two production systems is illustrated in Figure 1.

Life cycle databases and China-specific LCA modeling

Foreground data describe 2025 plant operations and include concentrate quantity and sourcing, grade, fuels, purchased electricity, oxygen and nitrogen, fluxes and auxiliary materials, product and sulfuric acid outputs, and transport. Missing or anomalous records were checked against company information, process balances, and literature parameters; complete inventories are reported in the Supplementary Materials [Supplementary Tables 2-5]. The 20,000 km maritime distance applied to imported concentrate in both routes is a primary foreground value reported by the participating plants rather than a generic default. We retained the plant-reported value because independently reconstructing an import-weighted distance would require additional assumptions regarding origin and destination ports, actual sailing routes, and transshipment patterns, for which sufficiently resolved records were unavailable. Such a reconstruction could therefore introduce greater uncertainty than the available primary operational data. Given the geographical proximity of the two plants, applying the same reported maritime distance to both cases was considered appropriate.

To assess the sensitivity of the results to the assumed maritime transport distance, an additional one-at-a-time sensitivity analysis was conducted for the double-flash case using the eBalance-CLCD-China 0.8.1 and eFootprint-CLCD-China 0.9 configurations. The baseline maritime distance of 20,000 km was varied by ±30%, corresponding to 14,000 km and 26,000 km. All other inventory parameters, including road transport distance, transport datasets, and economic allocation, were held constant. This scenario-based analysis evaluates the influence of distance uncertainty rather than reconstructing an import-weighted transport distance. Detailed calculations are provided in Supplementary Section 8.2 of the Supplementary Materials.

For electricity comparisons, purchased electricity is separated from electricity used to produce oxygen and nitrogen. Because 2.4% of plant electricity was supplied on site, relevant quantities were converted to a

purchased-electricity basis using a factor of 0.976. Oxygen- and nitrogen-production electricity was calculated at 0.65 and 0.12 kWh/Nm^3, respectively, with the 0.976 factor applied only once [Supplementary Tables 2 and 4].

Background datasets represent concentrate production, energy and fuel supply, auxiliary materials, transport, and waste treatment [Supplementary Tables 6-9]. China-specific datasets were preferred where available; global or other regional datasets were used otherwise. Previous comparative studies show that LCA software and background-database choices can affect both numerical results and comparative conclusions[25-28]. Because database coverage and proxy requirements differ here, the primary analysis treats each software-database combination as an integrated modeling configuration rather than assuming fully separable software and database effects.

For the ecoinvent-based imported-concentrate inventories, regional production datasets were weighted according to the imported mass shares of the corresponding sources. The weighted emission factor was calculated by multiplying each regional production factor by its mass share and summing the results [Supplementary Table 10]. Where grade conversion was required, the dry concentrate input was multiplied by its actual copper grade and divided by the background model's reference grade.

For Ausmelt, the actual dry imported-concentrate input was 2.639 t per tonne of cathode copper, with a copper grade of 25.35%. For double-flash, the corresponding input was 3.922 t, with a copper grade of 26.00%. Using the adopted reference grade of 29.63% Cu in the ecoinvent-based models, the equivalent inputs were approximately 2.258 and 3.442 t, respectively. These equivalent inputs were used for background concentrate-production calculations. Separately modeled maritime and road transport used the actual physical masses, rather than the grade-converted inputs. Economic allocation between cathode copper and sulfuric acid was applied afterward. This conversion aligned model inputs with the background dataset reference grade. It did not standardize the two plants' actual feed compositions or operating conditions. The CLCD-based configurations used an adopted reference copper grade of 25%, giving equivalent production inputs of approximately 2.676 t for Ausmelt and 4.079 t for double-flash. For comparison, their production factors were rescaled to the common reference grade of 29.63%. This rescaling changes the reporting basis, not the modeled production contribution. Factors on the common basis should therefore not be multiplied directly by the 25%-grade equivalent inputs [Supplementary Table 11].

SimaPro 10.1 uses ecoinvent 3.10 with the cut-off system model and the IPCC 2021 method for 100-year global warming potential (GWP100)[47-50], while OpenLCA 2.1 uses ecoinvent 3.11 with the same system model and impact-assessment method[51-53]. An additional OpenLCA model was reconstructed for the double-flash case using ecoinvent 3.10 inventory parameters exported from the corresponding SimaPro model, with the exported values rounded to three decimal places [Supplementary Table 12]. Because ecoinvent 3.10 was not imported natively into OpenLCA and linked independently, this comparison evaluates the numerical fidelity of model transfer under harmonized inputs rather than equivalence in native database linking and characterization. The test was limited to the double-flash case because its purpose was to assess transfer fidelity rather than compare the two production routes; the double-flash system also served as the benchmark for the subsequent database-version and decarbonization analyses. GaBi 10.6 uses the reduced-coverage Education Database 2020[54]; missing processes are supplemented with ecoinvent 3.11 proxies, so this configuration is treated as an illustrative reduced-coverage case. GaBi's imported-concentrate proxy uses the same mass-weighted regional ecoinvent 3.11 production datasets as OpenLCA. Neither configuration uses a global concentrate-market dataset to represent imported-concentrate supply. eFootprint and eBalance use CLCD-based Chinese data[55,56]. Unrepresented process emissions are added using IPCC methods and stoichiometric relationships. Because database families and proxy processes overlap across

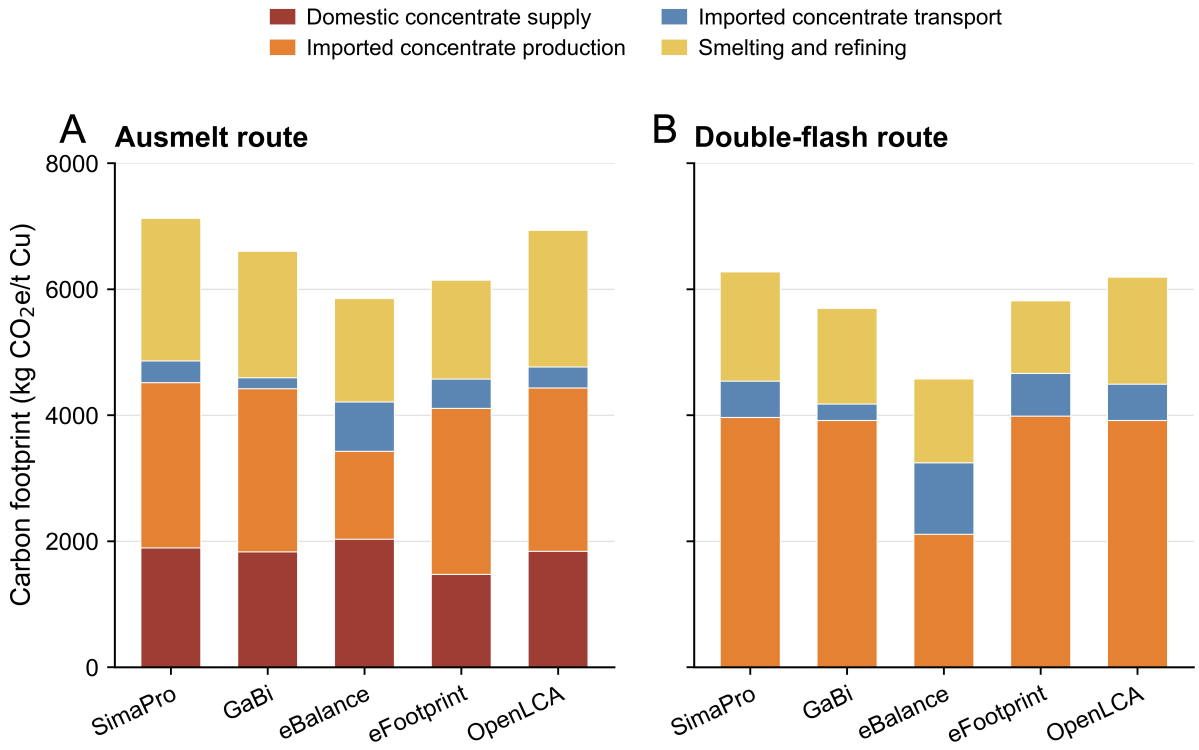


Figure 2. Life-cycle carbon footprint results for the Ausmelt case (A) and the double-flash case (B).

configurations, the five implementations are not statistically independent; dataset provenance is reported in the Supplementary Materials.

RESULTS AND DISCUSSION

Carbon footprints of refined copper from a coupled production-system perspective

Across the five configurations, the observed Ausmelt case has a cradle-to-gate carbon footprint of 5.9-7.1 t CO_2e/t Cu, compared with 4.6-6.3 t CO_2e/t Cu for the double-flash case; paired route differences range from 0.33 to 1.27 t CO_2e/t Cu [Figure 2]. The higher Ausmelt values reflect the sampled plant's supply chain and operating conditions, including domestic concentrate use and higher coal and electricity intensities. The comparison therefore concerns two coupled production systems rather than smelting technology in isolation. The contributions from domestic copper concentrate production in the Ausmelt case are detailed in Figure 3.

For the Ausmelt case, imported concentrate production contributes 24%-43% of the life-cycle footprint and its transport 3%-13%; the combined module contributes 37%-50%, with concentrate production consistently dominating logistics. The Ausmelt furnace contribution category accounts for 13%-19%, while domestic concentrate supply contributes approximately 24%-35%. The furnace category is narrower than the full smelting-and-refining boundary used in the section entitled "Comparison of emissions within a common smelting-and-refining boundary under observed feed and operating conditions".

For the double-flash case, concentrate mining and beneficiation contribute 46%-69% and associated transport 5%-25%, together accounting for 71%-80% of the life-cycle footprint. The upper transport share occurs in the eBalance-CLCD-China 0.8.1 configuration, in which sea and road transport contribute approximately 1.133 t CO_2e/t Cu after application of the copper-allocation factor of 0.9726, equivalent to 24.75% of the total footprint and rounded to 25%. This relatively high transport contribution should be

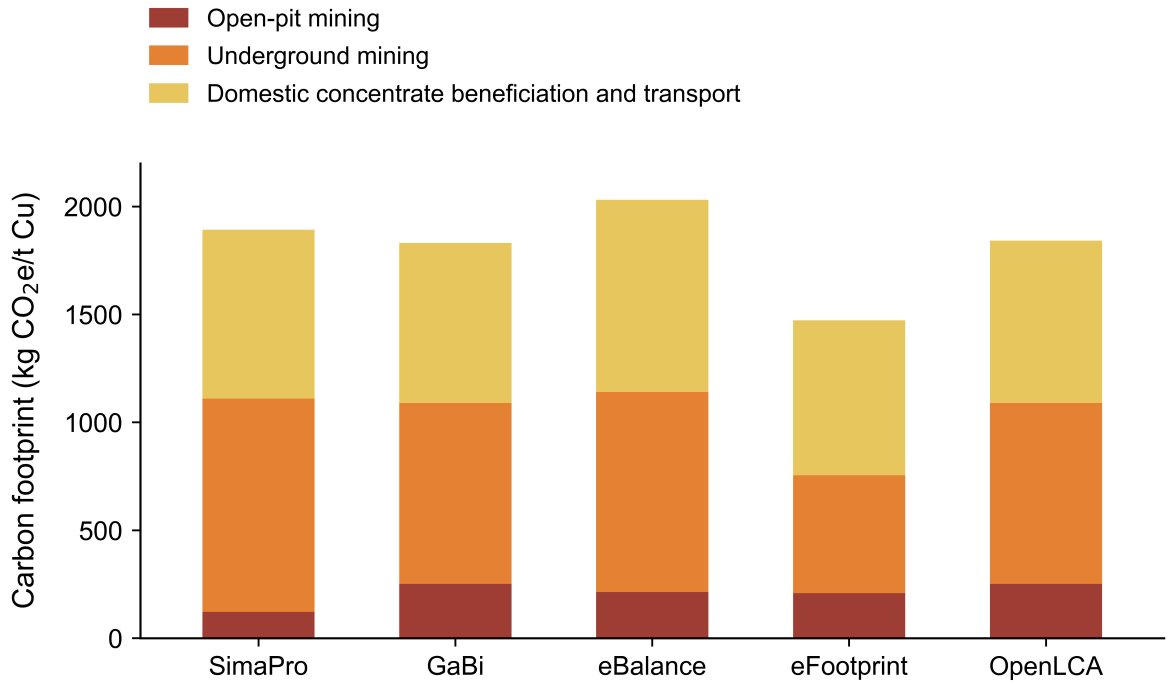


Figure 3. Carbon footprint results for the domestic copper concentrate used in the Ausmelt case. LCA: Life cycle assessment.

interpreted with caution. Both CLCD-based configurations employ a 2,500 t dry-bulk-carrier transport dataset, which is more representative of coastal or inland shipping than large ocean-going bulk carriers typically used for transoceanic concentrate transport. Consequently, the approximately 25% transport share in the eBalance configuration may partly reflect a mismatch between the selected transport proxy and the actual maritime transport conditions. The comparatively low concentrate-production burden and total footprint in this configuration further increase the proportional contribution of transport. This limitation highlights the importance of selecting transport datasets that adequately represent the vessel class and operating conditions of international concentrate shipments. Configuration spread is nevertheless driven mainly by background representations of concentrate production. On-site contributions are smaller: flash converting contributes about 8%-13%, largely through air-separation electricity, and sulfuric-acid production contributes 7%-9%. The upstream dominance is consistent with evidence that lower ore grades and greater comminution requirements can increase energy use and greenhouse-gas intensity in copper mining and beneficiation[57-61].

Despite different emission profiles, both cases point to the same broad mitigation priorities: lower-carbon concentrate supply, cleaner electricity, and higher process and air-separation efficiency. Figure 4 summarizes electricity-linked and fuel-combustion contributions for both cases in the SimaPro-ecoinvent 3.10 configuration.

Comparison of emissions within a common smelting-and-refining boundary under observed feed and operating conditions

Within the common smelting-and-refining boundary, the Ausmelt case is 1.57-2.26 t CO_2e/t Cu and double-flash 1.15-1.73 t CO_2e/t Cu, a difference of 0.31-0.53 t CO_2e/t Cu [Figure 5]. The boundary includes pretreatment, smelting, converting, anode-furnace refining, electrorefining, sulfuric-acid production, and oxygen- and nitrogen-production electricity, while excluding upstream concentrate production and transport.

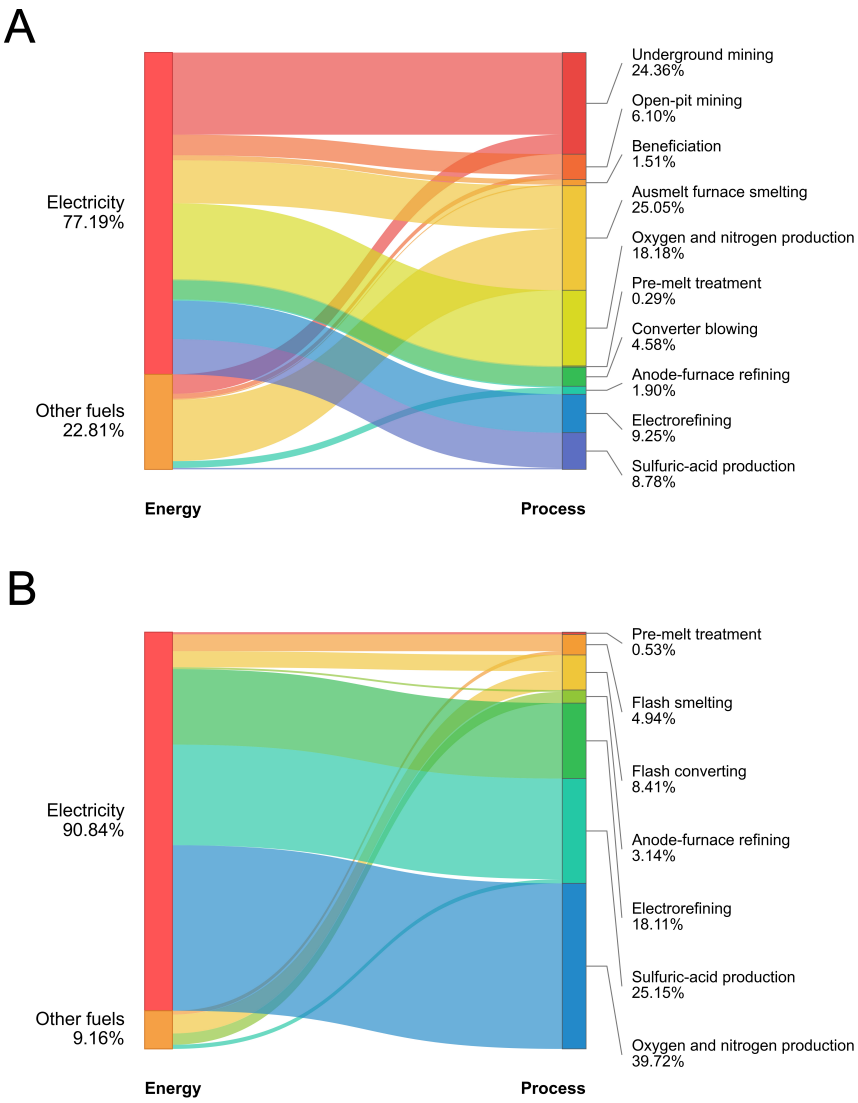


Figure 4. Energy-related flow contributions for the Ausmelt (A) and double-flash (B) cases. Flow widths show electricity-linked emissions and other fuel/direct-emission contributions before economic allocation. Where process-level fuel attribution was unavailable, the process distribution followed the available modeled shares, scaled to the total fuel emissions.

This remaining difference cannot be assigned to reactor type alone because the plants process different feeds [Table 3]. The Ausmelt case combines imported and domestic concentrates, has a lower input-mass-weighted copper grade, and has a lower acid-output-implied recovered-sulfur equivalent. The available data do not separate feed sulfur content from differences in sulfur capture or partitioning.

The Ausmelt case uses 142.8 kg raw coal/t Cu, whereas the double-flash case uses none. Direct purchased electricity excluding sulfuric-acid production is 848.8 kWh/t Cu for Ausmelt and 450.3 kWh/t Cu for double-flash. Sulfuric-acid-production electricity is 291.1 and 407.0 kWh/t Cu, respectively, giving total direct purchased-electricity demands of 1,139.9 and 857.3 kWh/t Cu. At sulfuric-acid outputs of 2.646 and 3.7 t H_2SO_4/t Cu, the acid-plant electricity intensity is 110.0 kWh/t H_2SO_4 in both cases. Oxygen- and nitrogen-production electricity is 623.9 versus 666.3 kWh/t Cu. Total electricity-related demand is therefore 1,763.8 versus 1,523.6 kWh/t Cu, a difference of 240.3 kWh/t Cu calculated using the unrounded values.

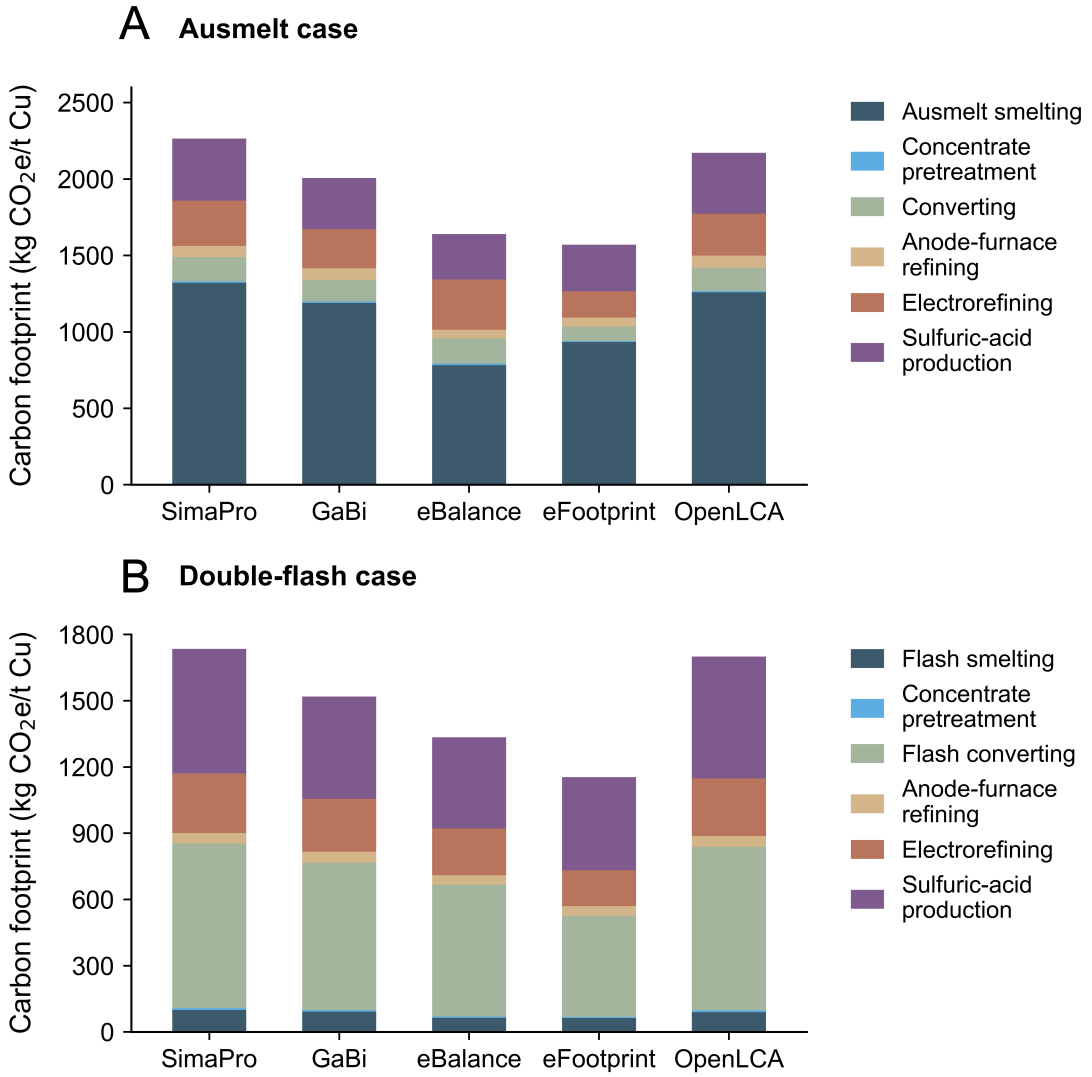


Figure 5. Carbon footprint results within the common smelting-and-refining boundary for the Ausmelt case (A) and the double-flash case (B). LCA: Life cycle assessment.

Table 3. Feed characteristics and sulfuric-acid outputs of the two observed production systems

Parameter	Ausmelt case	Double-flash case
Total concentrate input	4.354 t/t Cu	3.922 t/t Cu
Cu grade of imported concentrate	25.35%	26.00%
Cu grade of domestic concentrate	20.45%	/
Weighted-average Cu grade	23.42%	26.00%
Recovered sulfur equivalent derived from sulfuric acid output	0.865 t/t Cu	1.210 t/t Cu
Recovered sulfur equivalent relative to concentrate input	19.87%	30.84%

Sulfur values are recovered-sulfur equivalents inferred from sulfuric-acid output, not measured total sulfur contents. The calculation assumes 100% H_2SO_4-equivalent acid output and that recovered sulfur originates from the concentrate feed.

Because feed chemistry, operating practice, and process configuration were not normalized, the stage-level difference is interpreted as case-specific rather than as an intrinsic carbon advantage or penalty of either smelting technology. For context, Alexander *et al.*[30] reported 0.434-0.612 t CO_2e/t Cu for flash smelting plus Peirce-Smith converting and 0.678-0.703 t CO_2e/t Cu for side-blown smelting plus top-blown converting on

a concentrate-to-blister boundary. The higher stage-level values in the present study are not directly comparable because the boundary additionally includes anode-furnace refining, electrorefining, sulfuric-acid production, and air-separation electricity; the latter is a material energy demand in modern oxygen-enriched copper smelting[30].

Drivers of inter-configuration differences in refined copper carbon footprints

Inter-configuration divergence is concentrated in upstream concentrate supply and electricity [Figure 6A and B]. For the Ausmelt case, imported-concentrate production and transport vary by about 920 kg CO_2e/t Cu across configurations; for the double-flash case, the combined concentrate-production and transport module differs by approximately 1,420 kg CO_2e/t Cu between the eFootprint-CLCD-China 0.9 and eBalance-CLCD-China 0.8.1 configurations. After application of the common copper-allocation factor of 0.9726, eFootprint assigns approximately 1,876 kg CO_2e/t Cu more to concentrate production but approximately 457 kg CO_2e/t Cu less to transport than eBalance, yielding a net difference of 1,419.7 kg CO_2e/t Cu, reported as approximately 1,420 kg CO_2e/t Cu. The main drivers are assumptions about ore grade, mining and beneficiation technology, energy supply, transport, and system boundaries. Within the common smelting-and-refining boundary, electricity-related emissions range from 951.0 to 1,580.4 kg CO_2e/t Cu for Ausmelt and from 815.0 to 1,354.4 kg CO_2e/t Cu for double-flash [Supplementary Table 13]. Imported-concentrate factors and contributions are reported on different bases. Figure 6C shows production emission factors per kilogram of dry concentrate at the adopted common reference grade. Supplementary Tables 14 and 15 show production contributions per tonne of cathode copper before study-level economic allocation. These contributions use grade-converted background inputs, rather than the actual physical concentrate masses reported in Supplementary Tables 2 and 4. Figure 7 shows changes in the economically allocated cathode-copper footprint. Accordingly, dividing the contributions in Supplementary Tables 14 and 15 by the actual physical feed masses does not reproduce the reference-grade factors in Figure 6C. The calculation sequence and corresponding values are provided in Supplementary Tables 10 and 11.

All electricity factors in Supplementary Table 16 are life-cycle carbon-footprint factors, including the CLCD end-user datasets, but they differ in geographical scope, delivery level, background-modeling boundary, and temporal metadata. ecoinvent reports applicability intervals of 2021-2023 for version 3.10 and 2021-2024 for version 3.11[50,51]; for GaBi- and CLCD-based configurations, only database release or version years could be identified, so these dates are not treated as equivalent reference years.

Accordingly, the 0.550-0.914 kg CO_2e/kWh range reflects combined database and dataset-selection choices rather than a pure database-age effect. The 0.914 kg CO_2e/kWh ecoinvent 3.10 Central-China factor and the official 2024 national-average factor of 0.5777 kg CO_2e/kWh differ simultaneously in geography, delivery boundary, vintage, and background assumptions.

The eBalance-CLCD-China 0.8.1 configuration is retained as a legacy case relative to the 2025 foreground inventory. Its 2012 label denotes a database version or release year, not a verified reference year for every electricity process; the five-configuration range is therefore interpreted as an analytical envelope that includes a legacy implementation.

The controlled double-flash comparison evaluates the numerical fidelity of transferring a harmonized model between software environments. With the ecoinvent 3.10 inventory parameters, cut-off system model, economic-allocation procedure, and IPCC 2021 GWP100 method held constant, the SimaPro model and the OpenLCA reconstruction give 6.2748 and 6.2753 t CO_2e/t Cu, respectively. Their absolute difference is 0.0005 t CO_2e/t Cu, corresponding to 0.008% of the SimaPro result based on the unrounded values. This small residual is consistent with the three-decimal precision of the parameters exported from SimaPro and

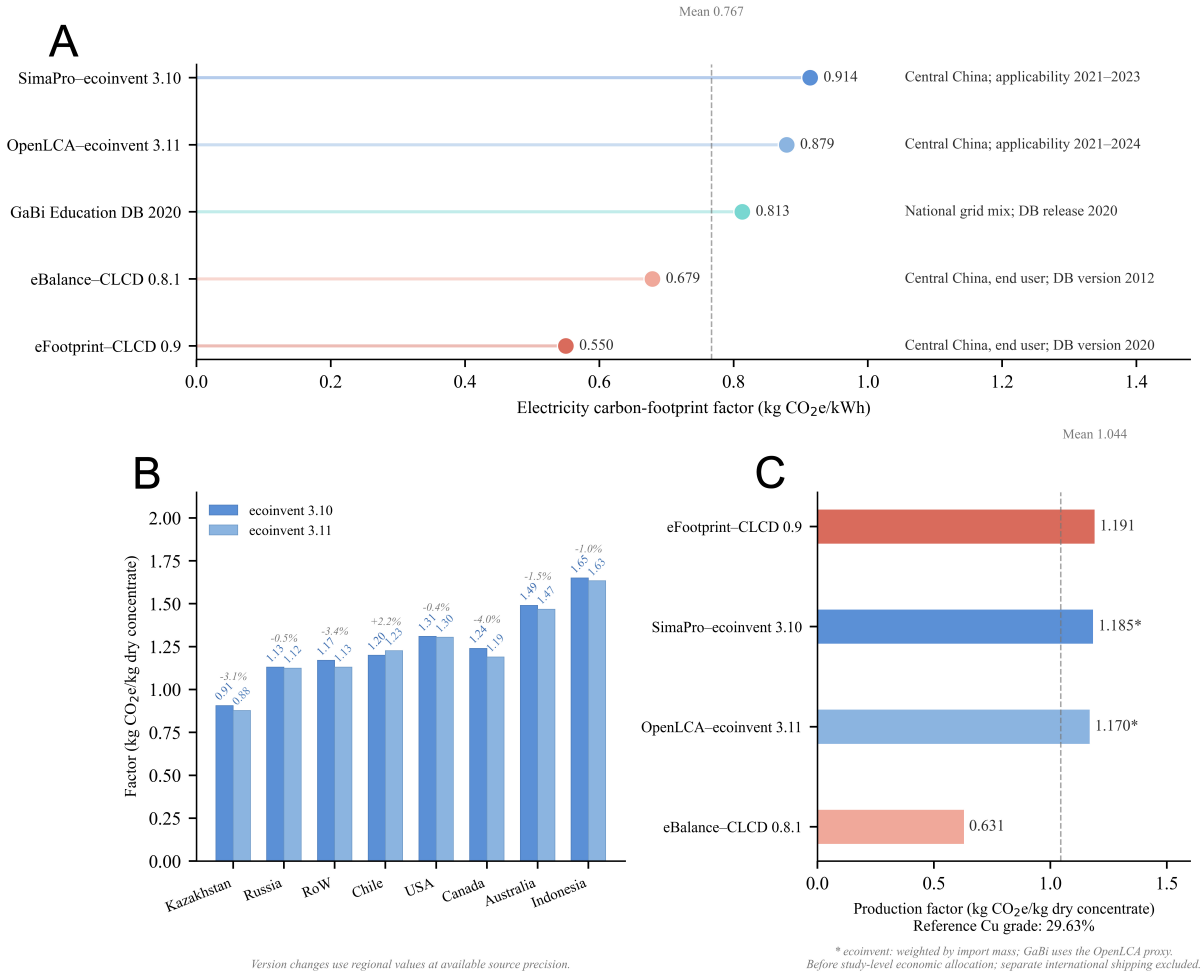


Figure 6. Differences in key background data among the software-database-modeling configurations. Panels (A-C) show electricity carbon-footprint factors, regional concentrate-production factors in ecoinvent 3.10 and 3.11, and weighted imported-concentrate production factors, respectively. Panel (C) reports imported-concentrate production factors on a common dry-mass basis at the adopted reference copper grade of 29.63%. These factors are reported before the study-level economic allocation between cathode copper and sulfuric acid. They exclude the separately modeled international shipping leg. GaBi uses the same ecoinvent 3.11 imported-concentrate proxy as OpenLCA. Background-dataset co-product treatment is retained. LCA: Life cycle assessment; DB: database; CLCD: Chinese Life Cycle Database; RoW: rest of the world.

indicates high transfer fidelity. The corresponding OpenLCA-ecoinvent 3.11 result is estimated at 6.193 t CO_2e/t Cu, 1.31% below the reconstructed ecoinvent 3.10 case; the Central-China electricity factor is also approximately 3.8% lower. Although ecoinvent 3.10 was not imported natively into OpenLCA and linked independently, and the comparison therefore does not establish equivalence in native database linking and characterization, the 0.008% residual shows that the numerical error introduced during model reconstruction was negligible relative to the broader inter-configuration differences observed in this study.

The five configurations are also not independent. Cross-database proxies account for 67.78% of the GaBi Ausmelt result and 70.01% of its double-flash result, mainly because ecoinvent 3.11 fills concentrate-mining and beneficiation gaps; proxy shares in the other configurations are 0%-2.19%. GaBi Education is therefore interpreted as an illustrative reduced-coverage configuration rather than an independent database family.

Excluding GaBi leaves the deterministic, economically allocated carbon-footprint ranges unchanged at 5,851-7,126 kg CO_2e/t Cu for Ausmelt and 4,578-6,275 kg CO_2e/t Cu for double-flash. Ausmelt remains higher in every retained, matched configuration. Thus, the deterministic comparison is not driven by the

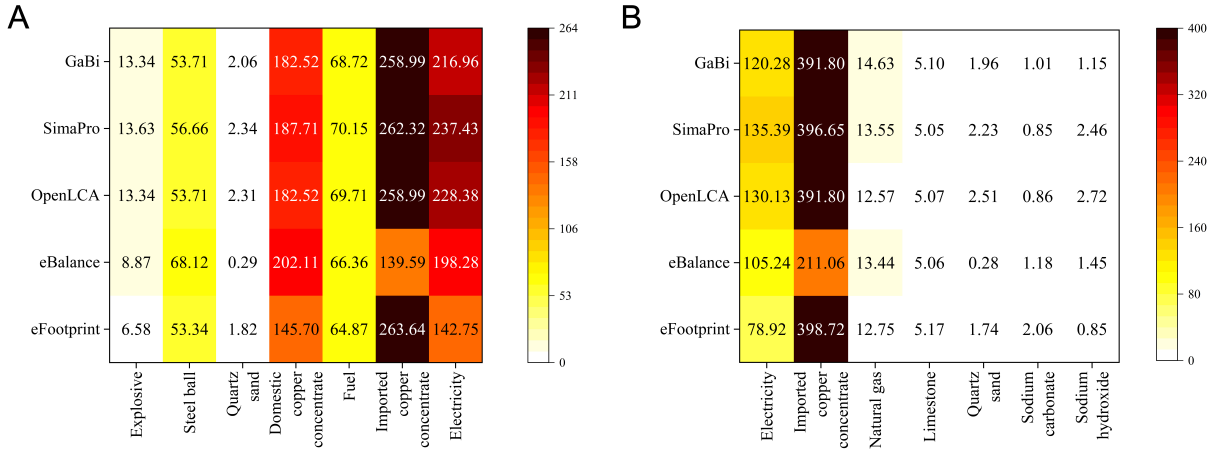


Figure 7. Route-specific sensitivity heat maps for the Ausmelt case (A) and the double-flash case (B). Parameter sets reflect the inventory structure of each route and are not intended for direct parameter-by-parameter comparison. Steel-ball and explosive inputs in panel (A) are disaggregated upstream inputs for domestic-concentrate mining and beneficiation, whereas analogous inputs are embedded in the imported-concentrate background process for the double-flash case. Values show absolute changes in the economically allocated cathode-copper footprint under one-at-a-time ±10% input changes. Imported-concentrate sensitivity is calculated from the grade-converted production contribution after economic allocation, not directly from the factor displayed in Figure 6C. LCA: Life cycle assessment.

reduced-coverage GaBi case.

The main data priority is therefore to develop localized, regularly updated inventories for concentrate mining and beneficiation, electricity supply, import transport, and major auxiliary materials. Better harmonization of these processes would improve cross-study comparability and industrial benchmarking.

Sensitivity analysis

Allocation sensitivity was evaluated for SimaPro-ecoinvent 3.10. Relative to base-case economic allocation (7.126 t CO_2e/t Cu for Ausmelt; 6.275 t CO_2e/t Cu for double-flash), assigning zero value to sulfuric acid increases the results by only 2.01% and 2.82%, respectively, indicating modest price sensitivity within economic allocation.

Changing the allocation principle has a much larger effect: mass allocation gives 1.994 and 1.373 t CO_2e/t Cu, while system expansion gives 6.976 and 6.041 t CO_2e/t Cu for Ausmelt and double-flash, respectively [Supplementary Table 17]. Despite these shifts, Ausmelt remains higher in all four scenarios, so the case-level ordering is not driven by the base-case allocation choice.

A separate one-at-a-time analysis perturbed selected inventory parameters by ±10%. Parameter sets follow each route's inventory structure and are therefore diagnostic rather than directly comparable between technologies. Steel balls and explosives, for example, are explicit in the disaggregated domestic-concentrate model for Ausmelt but embedded in the aggregated imported-concentrate dataset for double-flash.

For Ausmelt, imported concentrate and electricity are the most influential parameters. A ±10% change in imported-concentrate input changes the economically allocated footprint by 139.6-263.6 kg CO_2e/t Cu, while a 10% electricity change produces up to 237.4 kg CO_2e/t Cu. Domestic concentrate is the next-largest driver (145.7-202.1 kg CO_2e/t Cu), followed by fuel use; most auxiliary inputs have smaller effects.

For double-flash, imported concentrate and electricity again dominate: a ±10% change in imported-concentrate input changes the economically allocated footprint by 211.1-398.7 kg CO_2e/t Cu, while a 10% electricity reduction lowers it by 78.9-135.4 kg CO_2e/t Cu. Other fuel, flux, and reagent inputs have smaller effects.

Across both cases, sensitivity is concentrated in concentrate supply and electricity, reinforcing the importance of lower-carbon upstream production and improved electricity efficiency.

An additional sensitivity analysis was conducted to evaluate the influence of maritime transport distance on the carbon footprint of the double-flash case. The baseline distance of 20,000 km was varied by ±30%, while all other inventory parameters were held constant. For the eBalance-CLCD-China 0.8.1 configuration, the total carbon footprint ranged from 4,241.52 to 4,914.69 kg CO_2e/t Cu, compared with the baseline value of 4,578.11 kg CO_2e/t Cu, corresponding to a variation of ±7.35%. For eFootprint-CLCD-China 0.9, the corresponding carbon footprint ranged from 5,623.79 to 6,011.82 kg CO_2e/t Cu, compared with the baseline value of 5,817.81 kg CO_2e/t Cu, representing a variation of ±3.33%. The greater sensitivity observed for eBalance reflects its higher baseline maritime transport emissions. Nevertheless, the relative ranking of the two configurations remained unchanged across the examined distance scenarios. These results demonstrate that maritime distance assumptions affect the absolute carbon footprint estimates, while the extent of their influence depends on the background transport dataset. The detailed calculations are provided in Supplementary Table 18 of the Supplementary Materials.

Uncertainty analysis: within-configuration parameter uncertainty and inter-configuration dispersion

Two forms of variation are distinguished. Following established LCA uncertainty frameworks that separate parameter uncertainty from model- and choice-related variation[62,63], and the distinction between uncertainty within a realization and variation across alternative realizations[64], within-configuration uncertainty is defined as dispersion from uncertain inputs while a software-database-modeling structure is held fixed. Inter-configuration dispersion is the spread across implementations with different background databases, proxies, and embedded assumptions. Because only five non-independent configurations are examined, the latter is treated descriptively rather than as a population probability distribution.

Within-configuration uncertainty is evaluated for each foreground-background coupling. Plant-level flows are linked to their background unit processes and assessed for reliability, completeness, and temporal, geographical, and technological correlation [Supplementary Tables 19 and 20]. Background-data representativeness therefore affects the uncertainty assigned to each process contribution without changing model topology.

The five data-quality dimensions are adapted from the pedigree-matrix framework of Weidema and Wesnæs[65], with empirically based uncertainty factors developed by Ciroth *et al.*[66] and extensions to the distributions used in ecoinvent v3 described by Muller *et al.*[67]. In the present implementation, the numerical data quality indicator (DQI) scale is reverse-coded relative to the conventional Weidema-Wesnæs pedigree numbering: a score of 5 denotes the highest data quality or best representativeness, whereas a score of 1 denotes the lowest. The aggregated DQI scores are mapped to the bounded Beta distributions specified by Mo and Zhang[68]. For each deterministic process contribution x, the DQI determines a relative endpoint parameter p and symmetric Beta shape parameters $\alpha = \beta$; the sampling interval is defined as $[x(1 - p), x(1 + p)]$. Because the Beta distribution is symmetric and the bounds are centered on x, the expected value of each sampled contribution equals its corresponding deterministic value. The DQI therefore controls the dispersion around the deterministic contribution rather than shifting its expected value. This study retains this bounded Beta treatment rather than the lognormal treatment commonly used in ecoinvent; the resulting

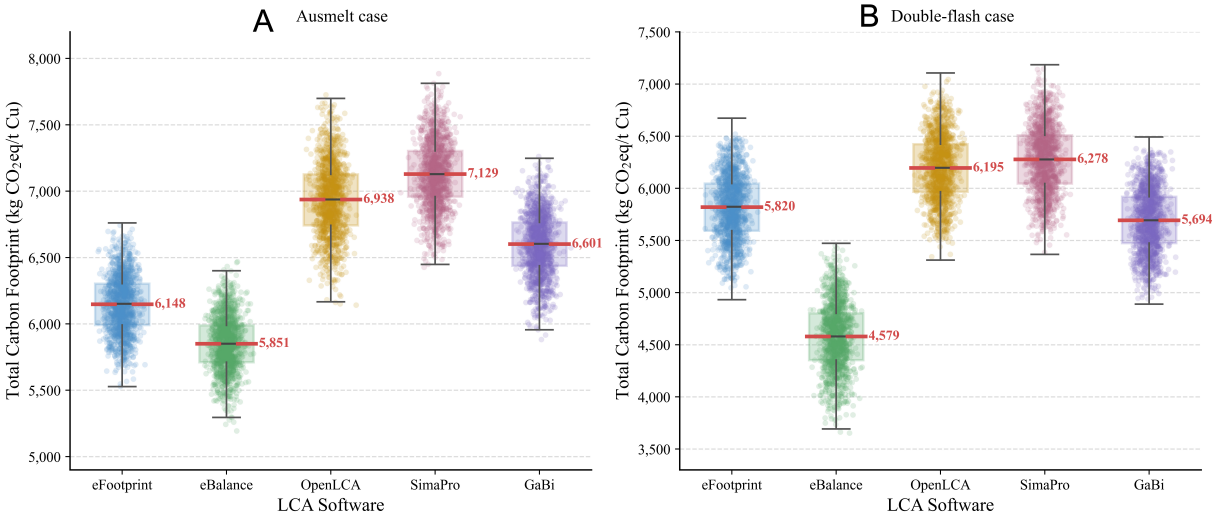


Figure 8. Monte Carlo distributions of the total carbon footprint for (A) the Ausmelt case and (B) the double-flash case. Each software-database configuration was evaluated using 10,000 Monte Carlo iterations, with common random numbers applied to homologous contributions for paired route comparisons. Boxes represent the 25th-75th percentiles, central horizontal lines denote medians, whiskers extend to the most extreme values within 1.5 times the interquartile range, and colored points show a fixed random subset of 1,400 realizations for visual clarity. Red dashed segments denote the simulated means, with the corresponding mean values shown adjacent to each box. All boxplot statistics and reported uncertainty metrics are based on the complete 10,000 simulations. LCA: Life cycle assessment.

intervals are therefore conditional on this distributional choice. The 95% interval uses the 2.5th and 97.5th percentiles, and interval-based relative uncertainty is defined as the interval half-width divided by the mean. For a like-for-like comparison between within-configuration parameter uncertainty and inter-configuration dispersion, however, both are expressed using the coefficient of variation (CV), defined as the standard deviation (SD) divided by the mean. Each configuration was propagated through 10,000 Monte Carlo iterations, with common random numbers applied to homologous contributions for paired route comparisons, following methodological discussions of Monte Carlo run numbers and dependent sampling in comparative LCA[69,70].

Because the stochastic calculations use the same finalized inventory and economic-allocation treatment as the deterministic calculations, and because each bounded Beta distribution is centered in expectation on the corresponding deterministic process contribution, the Monte Carlo means remain closely aligned with the deterministic estimates. Across all ten route-configuration combinations, the absolute relative difference is less than 0.06%.

Monte Carlo means range from 5,851 to 7,129 kg CO_2e/t Cu for Ausmelt and from 4,579 to 6,278 kg CO_2e/t Cu for double-flash. Interval-based relative within-configuration uncertainties are 6.58%-7.56% for Ausmelt and 9.53%-13.56% for double-flash, respectively [Supplementary Tables 21 and 22]; the wider double-flash intervals reflect its specific foreground-background couplings and DQI scores, not an intrinsic property of the technology. The corresponding Monte Carlo distributions are shown in Figure 8.

Paired Ausmelt-minus-double-flash differences range in mean from 328 to 1,272 kg CO_2e/t Cu, and all 95% paired intervals remain above zero [Supplementary Table 23]. Under the adopted DQI-Beta assumptions, these results indicate a positive mean difference for the two observed plant systems, but they do not imply that Ausmelt was higher in every paired realization. This establishes robustness for the two observed plant systems, not an intrinsic technology difference.

Table 4. Electricity-intensity trajectories under three stylized process-efficiency scenarios

Efficiency case	2025 (kWh/t Cu)	2030 (kWh/t Cu)	2035 (kWh/t Cu)	2050 (kWh/t Cu)	2060 (kWh/t Cu)
Conservative, 1.0% yr^{-1}	1,523.6	1,448.9	1,377.9	1,185.1	1,071.7
Moderate, 1.1% yr^{-1}	1,523.6	1,441.6	1,364.0	1,155.5	1,034.5
Accelerated, 1.2% yr^{-1}	1,523.6	1,434.3	1,350.3	1,126.6	998.5

Trajectories start from the observed 2025 demand of 1,523.6 kWh/t Cu and assume constant annual efficiency-improvement rates; they are sensitivity trajectories, not forecasts or physical lower bounds.

Across the five configuration means, the sample standard deviation is 533.3 kg CO_2e/t Cu for Ausmelt and 680.0 kg CO_2e/t Cu for double-flash, corresponding to inter-configuration CVs of 8.16% and 11.90%, respectively. For a like-for-like SD-based comparison, the within-configuration Monte Carlo distributions have CVs of 3.44%-3.95% for Ausmelt and 5.06%-7.00% for double-flash [Supplementary Tables 21 and 22]. The inter-configuration CV is therefore approximately 2.1-2.4 times the within-configuration CV for Ausmelt and 1.7-2.4 times that for double-flash. Thus, for both observed production systems, inter-configuration dispersion exceeds within-configuration parameter uncertainty. Because only five configurations are examined and the configurations are not statistically independent, these ratios are descriptive of the implementations considered rather than estimates of an underlying population distribution of structural uncertainty.

Differences in uncertainty width likewise reflect the fit between foreground flows and their background representations, not software performance or database quality. Important couplings include imported concentrate and air-separation electricity for double-flash and the mixture of domestic and imported concentrate, fuel use, and electricity demand for Ausmelt.

Reducing both forms of variation therefore requires better-matched background data and stronger empirical information on covariance among major inventory parameters.

Decarbonization potential of smelting and refining processes

Because electricity is an important on-site contributor, mitigation analysis focuses on the observed double-flash system and three levers: lower specific electricity demand, grid decarbonization, and improved oxygen-production efficiency. These are plant-level sensitivity scenarios, not forecasts for the Chinese copper industry. The assumed process-efficiency trajectories are summarized in Table 4.

The 2025 baseline electricity demand is 1,523.6 kWh/t Cu, including purchased electricity for pretreatment, smelting and converting, refining, sulfuric-acid production, and oxygen and nitrogen production. Upstream electricity embedded in concentrate production and transport is excluded. A detailed reconciliation is provided in the Supplementary Materials.

The primary calibration baseline is the official 2024 national-average life-cycle electricity carbon-footprint factor of 0.5777 kg CO_2e/kWh[71]. The factor calculated from the projected 2025 generation shares in Table 5 is 0.5364 kg CO_2e/kWh. Adding the official transmission-and-distribution component of 0.0327 kg CO_2e/kWh, including network losses, to the projected generation-mix factor gives 0.5691 kg CO_2e/kWh, leaving a residual difference of 0.0086 kg CO_2e/kWh, or approximately 1.5% of the official 2024 factor, associated with the difference between the projected 2025 and actual 2024 generation mixes. To ensure internal consistency, the entire modeled trajectory was proportionally adjusted to match the selected 2025 baseline. The primary analysis uses 0.5777 kg CO_2e/kWh, while 0.550 and 0.914 kg CO_2e/kWh are examined as alternative baselines in the sensitivity analysis [Supplementary Table 24].

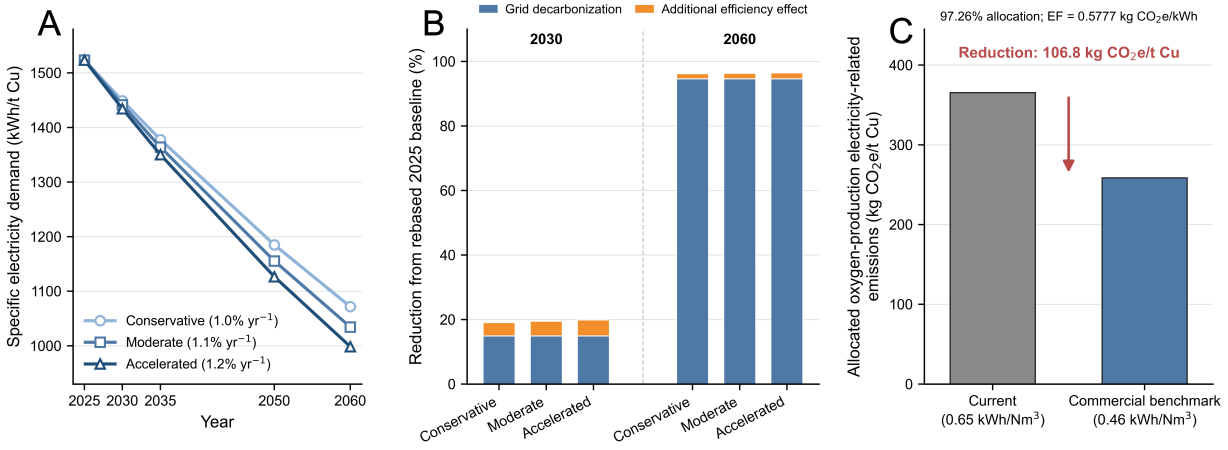


Figure 9. Electricity-related mitigation analysis for the double-flash case: (A) specific electricity-demand trajectories under the three efficiency scenarios; (B) grid-only and additional process-efficiency contributions to modeled emission reductions in 2030 and 2060 relative to the consistently rebased 2025 electricity-factor baseline of 0.5777 kg CO_2e/kWh; and (C) economically allocated oxygen-production emissions at 0.65 and 0.46 kWh/Nm³ under a common electricity factor. EF: Emission factor.

Table 5. Technology-specific electricity carbon footprint factors and projected national generation mix[72]

Generation technology	2024 factor (kg CO_2e/kWh)	Share in 2025	Share in 2030	Share in 2035	Share in 2050	Share in 2060
Coal	0.924	0.54	0.44	0.30	0.01	0
Coal + CCS	0	0	0	0.03	0.09	0.05
Gas	0.4503	0.06	0.08	0.11	0.03	0
Gas + CCS	0	0	0	0	0.03	0.03
Nuclear	0.0065	0.05	0.06	0.08	0.13	0.15
Hydro	0.0141	0.15	0.14	0.13	0.13	0.13
Wind	0.0324	0.11	0.14	0.18	0.28	0.31
Solar PV	0.052	0.07	0.12	0.16	0.28	0.31
Biomass	0.0404	0.02	0.02	0.01	0	0
Biomass + CCS	0	0	0	0	0.02	0.02

The 2025-2060 columns report projected generation shares. The directly weighted factors combine these shares with technology-specific life-cycle factors. Because the resulting 2025 weighted factor of 0.5364 kg CO_2e/kWh differs in year and delivery boundary from the official 2024 national-average factor of 0.5777 kg CO_2e/kWh, the scenario trajectory is rebased to the selected 2025 calibration factor before mitigation percentages are calculated. Generation shares are from Zhuo *et al.*[72], technology factors are from the official 2024 Chinese dataset[71], and CCS generation is assigned zero only as an idealized lower-bound assumption. CCS: Carbon capture and storage; PV: photovoltaic.

Three stylized process-efficiency trajectories assume annual reductions in specific electricity demand of 1.0%, 1.1%, and 1.2% for the conservative, moderate, and accelerated cases, respectively. These are sensitivity trajectories for 2025-2060, not forecasts or physical lower bounds; no regulatory or engineering minimum is imposed. The resulting pathways are shown in Table 4 and Figure 9A.

$$I_{s,t} = I_{2025}(1 - r_s)^{t-2025} \quad (1)$$

where I_{2025} is the observed 2025 demand, r_s is the annual efficiency-improvement rate, and t is the target year.

The electricity-supply trajectory is modeled independently of process efficiency. National generation shares for 2025-2060 are taken from Zhuo *et al.*[72], and technology-specific life-cycle factors from the officially published 2024 Chinese electricity carbon-footprint dataset[71]. Recent provincial life-cycle projections

likewise show substantial long-term declines and strong spatial heterogeneity in Chinese grid carbon-footprint factors through 2060[73], supporting the use of a decarbonizing-grid sensitivity trajectory while underscoring that the present national pathway is scenario-dependent. Because official factors for generation with carbon capture and storage (CCS) were unavailable, coal, natural gas, and biomass with CCS are assigned zero as an idealized net-zero lower bound rather than a measured commercial value.

The generation-weighted factors calculated directly from the projected electricity mixes are 0.5364, 0.4565, 0.3436, 0.0491, and 0.0290 kg CO_2e/kWh for 2025, 2030, 2035, 2050, and 2060, respectively. After rebasing the trajectory to the primary baseline of 0.5777 kg CO_2e/kWh, the factors used in the mitigation calculations are 0.5777, 0.4917, 0.3701, 0.0528, and 0.0312 kg CO_2e/kWh, respectively.

Three counterfactuals separate the mitigation mechanisms: grid only (2025 electricity demand with year-specific grid factors), efficiency only (declining demand with a fixed calibration factor), and combined (both change). The decomposition is used for attribution rather than implying that percentage reductions are directly additive; calculation equations are provided in the Supplementary Materials.

For each baseline-factor case, the year-specific electricity-factor trajectory is first rebased to the corresponding 2025 baseline. Percentage reductions are then evaluated against the consistently matched 2025 baseline emissions; full equations are provided in the Supplementary Materials.

Relative to the consistently rebased 2025 baseline, grid decarbonization alone reduces electricity-related emissions by 14.9% in 2030 and 94.6% in 2060. Including process-efficiency improvement increases the reductions to 19.1%-19.9% in 2030 and 96.2%-96.5% in 2060 [Figure 9B]. Grid decarbonization therefore accounts for 74.9%-78.1% of the combined 2030 reduction, while process efficiency contributes an additional 1.6-1.9 percentage points by 2060. Long-term mitigation is thus dominated by power-sector decarbonization.

When each electricity-factor trajectory is consistently rebased to its corresponding 2025 baseline, the percentage reductions are independent of the absolute baseline factor: combined reductions are 19.1%-19.9% in 2030 and 96.2%-96.5% in 2060 for all three baseline cases. The baseline factor affects absolute electricity-related emissions and the absolute benefit of oxygen-efficiency improvement, but switching between baseline datasets is not counted as mitigation. The long-term result remains conditional on the idealized zero-factor assumption for CCS generation [Table 5]. An illustrative sensitivity assigning life-cycle factors of 0.15 and 0.10 kg CO_2e/kWh to coal and natural gas generation with CCS, respectively, while retaining the zero factor for biomass with CCS, increases the directly weighted 2060 grid factor from 0.0290 to 0.0395 kg CO_2e/kWh and reduces the grid-only emission reduction from 94.6% to 92.6% (approximately 93%).

For oxygen production, the double-flash inventory reports a physical oxygen demand of 1,025.37 Nm^3 O_2/t Cu. For electricity accounting, this physical demand is converted to a purchased-electricity-equivalent oxygen demand of 1,000.76 Nm^3 O_2/t Cu (1,025.37 × 0.976; 0.976 is the share of electricity purchased from the grid) at 0.65 kWh/Nm^3. A benchmark of 0.46 kWh/Nm^3 was derived from the unit-energy parameter of 321 kWh/t O_2 reported by Coursol *et al.* for tonnage-oxygen production at 600 kPa[74]. For comparability, the observed and benchmark electricity intensities were assumed to represent 99.6% oxygen delivered at the same pressure. The oxygen purity is therefore an explicit plant-matching assumption rather than a specification directly reported in the cited source.

At the 2024 national-average electricity factor, reducing oxygen-production electricity from 0.65 to 0.46 kWh/Nm^3 saves 190.1 kWh/t Cu on a purchased-electricity-equivalent basis and avoids 106.8 kg CO_2e/t Cu after economic allocation (109.8 kg CO_2e/t Cu before economic allocation) [Figure 9C].

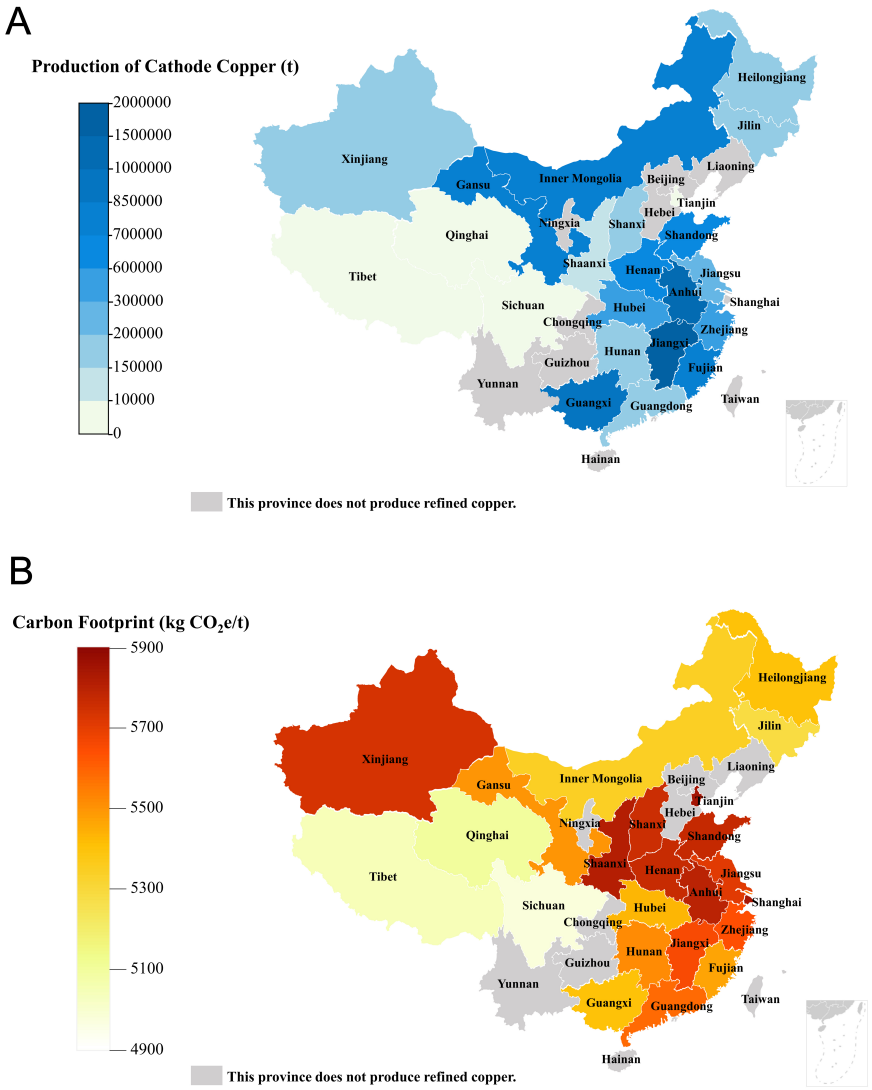


Figure 10. Spatial distribution of (A) annual cathode-copper production in China in 2022 and (B) the modeled cradle-to-gate carbon footprint of refined copper under province-specific electricity-factor scenarios (kg CO_2e/t). Production data for panel (A) were obtained from the China Nonferrous Metals Industry Yearbook 2023[21]. Panel (B) uses the revised double-flash SimaPro-ecoinvent 3.10 baseline, with provincial electricity factors estimated from normalized projected installed-capacity shares and technology-specific life-cycle electricity factors. Other inventory contributions are held constant. The results represent electricity-mix sensitivity scenarios rather than measured provincial production footprints. Base map: Standard Map Service of the Ministry of Natural Resources of China, approval no. GS(2022)4309 (https://bzdt.ch.mnr.gov.cn/); boundaries were not modified.

The avoided emissions are 101.7-169.0 kg CO_2e/t Cu after economic allocation across the Supplementary Table 16 factor range and decline as the grid decarbonizes; they are therefore not added directly to future grid-decarbonization reductions.

Figure 10A shows provincial cathode-copper production in China in 2022. For the regional sensitivity analysis in Figure 10B, provincial carbon footprints were recalculated by substituting province-specific electricity carbon-footprint factors into the revised double-flash SimaPro-ecoinvent 3.10 reference result, while keeping all other inventory contributions and economic-allocation settings unchanged. The baseline carbon footprint was 6,274.8 kg CO_2e/t Cu, with an electricity-equivalent demand of 1,523.554 kWh/t Cu, an electricity carbon-footprint factor of 0.914 kg CO_2e/kWh, and a copper economic-allocation fraction of 0.9726.

Province-specific electricity factors were estimated using the projected 2025 installed capacities of seven generation technologies derived from Zhuo *et al.*[72] and the technology-specific life-cycle electricity carbon-footprint factors reported in the official 2024 Chinese dataset[71]. The installed-capacity shares were recalculated and normalized to sum to unity within each province.

The provincial carbon footprints were then obtained by substituting the province-specific electricity factors for the explicitly modeled electricity demand, while keeping the remaining foreground and background inventory contributions and economic-allocation settings unchanged. This calculation gives a fixed residual contribution of 4,920.36 kg CO_2e/t Cu, which represents the lower bound under the hypothetical elimination of the explicitly modeled electricity-related emissions.

The recalculated provincial carbon footprints range from 4,947.6 to 5,833.2 kg CO_2e/t Cu across the 31 provincial electricity scenarios, and all values remain above this lower bound. These results represent an electricity-factor sensitivity analysis rather than independently simulated provincial production systems. Because the electricity factors are based on projected installed-capacity shares rather than measured electricity generation or provincial consumption mixes, the spatial results should be interpreted as screening-level estimates rather than actual provincial copper-production carbon footprints. Detailed calculations and consistency checks are provided in Supplementary Section 10.3 and Supplementary Table 25 of the Supplementary Materials.

Limitations and future work

Three limitations are central. First, several upstream processes rely on commercial databases, proxies, or indirectly estimated parameters, so differences in temporal, geographical, technological, and electricity-delivery coverage affect both absolute results and comparability. The configurations also share database families and proxies; in GaBi Education, proxies contribute 67.78% of the Ausmelt result and 70.01% of the double-flash result. Configuration statistics therefore describe the implementations examined, not a population distribution of structural uncertainty. Maritime transport modeling introduces additional uncertainty because the 2,500 t dry-bulk-carrier proxies used in the CLCD configurations may not adequately represent ocean-going concentrate shipments. Furthermore, the reported 20,000 km maritime distance could not be independently verified against import-weighted shipping routes. Although the distance sensitivity analysis quantifies the influence of a ±30% distance variation, it does not resolve the potential bias associated with vessel-class representativeness. Additionally, water sources and supply processes were not specified by the participating plants. Consequently, no separate water-supply process was modeled. Although water as an unprocessed natural-resource flow has zero direct GWP100 contribution, potential emissions from abstraction, pumping, treatment, and delivery remain unquantified.

Second, each production system is represented by one plant. Feed composition, concentrate sourcing, operating conditions, and technology choice covary in practice, so route differences cannot be generalized as technology effects. Isolating such effects would require normalization with a validated mass-and-energy-balance model or matched data from multiple plants. End-of-life recycling, secondary copper, and recovery of associated metals are also outside the cradle-to-gate boundary.

Third, one-at-a-time sensitivity analysis does not capture nonlinear interactions or covariance, and empirical covariance data were unavailable for Monte Carlo sampling. Future work should expand plant and temporal coverage, improve localized upstream inventories, validate concentrate composition and air-separation electricity use, and develop empirically supported dependency structures for uncertain life cycle inventory (LCI) parameters. Future inventories should document water sources and the energy and treatment required for water supply to enable consistent modeling across configurations.

Secondary copper is a particularly important extension because its carbon footprint can be substantially lower than primary production[33]. Including secondary production and recycling shares would enable system-level decarbonization analysis beyond primary pyrometallurgy.

CONCLUSIONS

Using 2025 operational data from two Chinese smelters, this study develops cradle-to-gate inventories for two primary refined-copper production systems and evaluates them across five software-database-modeling configurations, complemented by allocation sensitivity, a controlled parameter-transfer check using ecoinvent 3.10 inputs, paired uncertainty analysis, and electricity-related mitigation scenarios.

The observed Ausmelt case is higher than double-flash in all five configurations (5.9-7.1 versus 4.6-6.3 t CO_2e/t Cu). The difference reflects the sampled plants' feed and supply-chain structures and energy inputs, particularly domestic-concentrate use, coal, and electricity. Upstream concentrate production is a major contributor in both systems and the dominant source of inter-configuration divergence. Because feed composition and operating conditions were not normalized, the stage-level difference is case-specific rather than an intrinsic technology effect.

Configuration choice also affects absolute results. Under harmonized ecoinvent 3.10 inventory inputs and modeling settings, the OpenLCA reconstruction reproduced the corresponding SimaPro result within 0.008%, indicating high numerical fidelity of the parameter transfer and model reconstruction. Because the ecoinvent 3.10 database was not imported natively into OpenLCA and its processes were not linked independently, this check does not establish equivalence between the two programs in their native linking or characterization of ecoinvent. Based on the transferred inventory, the OpenLCA-ecoinvent 3.11 result was estimated at 6.193 t CO_2e/t Cu, 1.31% below the reconstructed ecoinvent 3.10 case. This comparison does not isolate a database-version effect. Within the study setup, this difference between ecoinvent configurations is substantially larger than the residual numerical difference introduced during model transfer. For a like-for-like SD-based comparison, the within-configuration Monte Carlo CVs are 3.44%-3.95% for Ausmelt and 5.06%-7.00% for double-flash, whereas the CVs across the five configuration means are 8.16% and 11.90%, respectively. Inter-configuration dispersion therefore exceeds within-configuration parameter uncertainty for both observed systems, by approximately 2.1-2.4 times for Ausmelt and 1.7-2.4 times for double-flash. Given the small number of configurations (n = 5) and their non-independence, this comparison is descriptive of the implementations examined rather than a population-level estimate of structural uncertainty.

For the observed double-flash system, modeled electricity-related mitigation is dominated by grid decarbonization. After consistently rebasing the electricity-factor trajectory to the official national-average baseline, combined reductions are 19.1%-19.9% in 2030 and 96.2%-96.5% in 2060. Reducing oxygen-production electricity from 0.65 to 0.46 kWh/Nm^3 avoids 106.8 kg CO_2e/t Cu after economic allocation (109.8 kg CO_2e/t Cu before economic allocation) at the same baseline. Deep decarbonization therefore requires coordinated action across concentrate supply, plant efficiency, air separation, and electricity supply.

Allocation strongly affects absolute footprints, but the Ausmelt case remains higher under all four SimaPro-ecoinvent 3.10 allocation scenarios. Transparent reporting of co-product treatment is therefore essential for comparison across studies.

More broadly, comparable refined-copper carbon footprints require localized, regularly updated background data and wider plant coverage. Future assessments should better control feed composition and operating conditions and incorporate empirically supported dependencies among uncertain inventory parameters.

DECLARATIONS

Acknowledgments

We thank China Nonferrous Metal Mining (Group) Co., Ltd. (CNMC), drawing on its industry expertise, CNMC offered general advice on survey approaches and potential sources of primary data. CNMC had no role in the research design, data, analysis, or manuscript preparation.

Authors' contributions

Methodology, data curation, software, writing - original draft: Shi, S.; Zhang, Z.; Luo, Q.
Conceptualization, methodology, software, writing - review and editing: Peng, T.
Conceptualization, writing - review and editing: Dong, W.
Investigation: Hou, Z.
Data curation: Hou, C.

Availability of data and materials

The original contributions presented in this study are included in the article/Supplementary Materials. Further inquiries can be directed to the corresponding author.

AI and AI-assisted tools statement

During the preparation of this manuscript, the AI tool ChatGPT (version GPT-5.6 Sol, released 2026-07-09) was used for language editing and for generating some small icons in the Graphical Abstract. These icons are decorative only and do not represent or alter any scientific data or findings. The overall design, layout, and scientific content of the Graphical Abstract were conceived and assembled by the authors. The tool did not influence the study design, data collection, analysis, interpretation, or the scientific content of the work. All authors take full responsibility for the accuracy, integrity, and final content of the manuscript.

Financial support and sponsorship

This work was supported by Envision Group, the Tsinghua University-Toyota Research Center (Grant Nos. TT-2025-04 and TT-2026-04), and the Tsinghua University Student Research Training (SRT) Project (Grant No. 2611T0904).

Conflicts of interest

All authors declared that there are no conflicts of interest.

Ethical approval and consent to participate

Not applicable.

Consent for publication

Not applicable.

Copyright

© The Author(s) 2026.

Supplementary Materials

Supplementary Materials

REFERENCES

1. Zhang, N. Analysis of supply and demand status and trend of copper resources in China under development background of new energy industry. *China. Min. Mag.* **2023**, *32*, 2-9. (in Chinese). DOI
2. Zhu, Y. G.; Zhang, W. F.; Wang, D.; Dou, S. Q.; Xu, D. Y. Resilience evaluation of China's copper resources industrial chain and supply chain. *Resour. Sci.* **2023**, *45*, 1761-77. (in Chinese). DOI
3. Implementation plan for the high-quality development of the copper industry (2025-2027) (MIIT Joint Raw Materials [2025] No. 18); Ministry of Industry and Information Technology of the People's Republic of China, 2025. (in Chinese) https://www.gov.cn/zhengce/zhengceku/202502/content_7003485.htm (accessed 2026-11-06).
4. Lu, Y.; Li, H. J. Review of research on the copper industrial chain. *Resour. Ind.* **2020**, *22*, 60-8. (in Chinese). DOI

5. Mi, X.; Lou, H.; Xie, H.; Mo, Y.; Zhang, W.; Xiang, C. Development strategy for advanced copper-based materials in China. *Chin. J. Eng. Sci.* **2023**, *25*, 96-103. (in Chinese). DOI
6. Li, Y.; Lin, W.; Wang, Z.; Miao, B.; Lin, G. Research status and trends of high-performance copper processing materials for new energy vehicles. *Copper. Eng.* **2025**, *6*, 85-109. (in Chinese). DOI
7. Liang, S. S.; Lv, X. Q. Research on the evolution of supply and consumption patterns of copper resources around the world and the influencing factors of copper consumption in China. *China. Min. Mag.* **2025**, *34*, 324-32. (in Chinese). DOI
8. Hao, M.; Wang, P.; Chen, W. Q. Copper resource demand prediction for low-carbon transition of China's power system. *Resour. Sci.* **2025**, *47*, 1449-61. (in Chinese). DOI
9. Lin, B. L.; Yan, W. D.; Guo, J.; Su, Y.; Yu, J. W. Prospects of global copper supply and demand during the 14th Five Year Plan Period. *China. Min. Mag.* **2021**, *30*, 16-22. (in Chinese). DOI
10. Kuipers, K. J.; van Oers, L. F.; Verboon, M.; van der Voet, E. Assessing environmental implications associated with global copper demand and supply scenarios from 2010 to 2050. *Glob. Environ. Change.* **2018**, *49*, 106-15. DOI
11. Elshkaki, A.; Graedel, T.; Ciacci, L.; Reck, B. K. Copper demand, supply, and associated energy use to 2050. *Glob. Environ. Change.* **2016**, *39*, 305-15. DOI
12. Van der Voet, E.; Van Oers, L.; Verboon, M.; Kuipers, K. Environmental implications of future demand scenarios for metals: methodology and application to the case of seven major metals. *J. Ind. Ecol.* **2019**, *23*, 141-55. DOI
13. Watari, T.; Nansai, K.; Nakajima, K. Major metals demand, supply, and environmental impacts to 2100: a critical review. *Resour. Conserv. Recycl.* **2021**, *164*, 105107. DOI
14. Liu, H. X.; Wu, L. M.; Lin, Q. Y.; et al. Carbon-footprint assessment technologies and their application in key industrial sectors. *Chem. Ind. Eng. Prog.* **2023**, *42*, 2201-18. (in Chinese). DOI
15. Wang, M. C.; Chen, R. Y. Impacts of China's carbon-peaking and carbon-neutrality goals on the domestic copper industry. *China. Nonferrous. Metall.* **2021**, *50*, 1-4. (in Chinese). DOI
16. Zhu, X. H.; Li, S. M.; Zeng, A. Q. A review and prospect of research on carbon emissions from the critical metal industry chain under clean energy transition. *Resour. Sci.* **2023**, *45*, 1-17. (in Chinese). DOI
17. Zhang, X. Y.; Wang, H. B.; Ma, H. Paths and methods for achieving carbon peaking and carbon neutrality in the copper industry. *Min. Metall.* **2024**, *33*, 456-65. (in Chinese). DOI
18. Chen, J. J.; Li, L. Q.; Li, B.; Wu, Y. F.; Zuo, T. Y. Current applications and development trends of LCA in the copper industry. *Mater. Rep.* **2017**, *31*, 357-62. (in Chinese). https://www.cnki.com.cn/Article/CJFDTotal-CLDB2017S2080.htm (accessed 2026-11-11).
19. Huang, J.; Deng, S. Y.; Ma, X. T.; Yang, J. Y. Current development and recommendations for the global copper industry. *Mod. Min.* **2021**, *37*, 1-5. (in Chinese). DOI
20. Zhang, N.; Liu, R. X. New trends in China's nonferrous metal mining industry under the dual-carbon and dual-circulation strategies. *China. Nonferrous. Met.* **2022**, *21*, 38-41. (in Chinese). DOI
21. China Nonferrous Metals Industry Association. China nonferrous metals industry yearbook 2023; Metallurgical Industry Press, 2024. (in Chinese) https://data.cnki.net/yearBook/single?id=8GryeNWB8SrlALlV8Xoj2w==&pinyinCode=YZGYA (accessed 2026-11-11).
22. Finnveden, G.; Hauschild, M. Z.; Ekvall, T.; et al. Recent developments in life cycle assessment. *J. Environ. Manage.* **2009**, *91*, 1-21. DOI
23. Nuss, P.; Eckelman, M. J. Life cycle assessment of metals: a scientific synthesis. *PLoS. One.* **2014**, *9*, e101298. DOI
24. Herrmann, I. T.; Moltesen, A. Does it matter which life cycle assessment (LCA) tool you choose? - a comparative assessment of SimaPro and GaBi. *J. Clean. Prod.* **2015**, *86*, 163-9. DOI
25. Speck, R.; Selke, S.; Auras, R.; Fitzsimmons, J. Choice of life cycle assessment software can impact packaging system decisions. *Packag. Technol. Sci.* **2015**, *28*, 579-88. DOI
26. Takano, A.; Winter, S.; Hughes, M.; Linkosalmi, L. Comparison of life cycle assessment databases: a case study on building assessment. *Build. Environ.* **2014**, *79*, 20-30. DOI
27. Martínez-Rocamora, A.; Solís-Guzmán, J.; Marrero, M. LCA databases focused on construction materials: a review. *Renew. Sustain. Energy. Rev.* **2016**, *58*, 565-73. DOI
28. Silva, D. A. L.; Nunes, A. O.; Moris, V. A. S.; Piekarski, C. M.; Rodrigues, T. O. How important is the LCA software tool you choose? Comparative results from GaBi, openLCA, SimaPro and Umberto. In *Proceedings of the VII Conferencia Internacional de Análisis de Ciclo de Vida en Latinoamérica*, 2017. https://www.researchgate.net/publication/318217178 (accessed 2026-11-11).
29. Sanjuan-Delmás, D.; Alvarenga, R. A. F.; Lindblom, M.; et al. Environmental assessment of copper production in Europe: an LCA case study from Sweden conducted using two conventional software-database setups. *Int. J. Life. Cycle. Assess.* **2022**, *27*, 255-66. DOI
30. Alexander, C.; Johto, H.; Lindgren, M.; Pesonen, L.; Roine, A. Comparison of environmental performance of modern copper smelting technologies. *Clean. Environ. Syst.* **2021**, *3*, 100052. DOI

31. Liu, L.; Xiang, D.; Cao, H.; Li, P. Life cycle energy consumption and GHG emissions of the copper production in China and the influence of main factors on the above performance. *Processes* **2022**, *10*, 2715. DOI
32. Lu, T.; Tikana, L.; Herrmann, C.; Ma, Y.; Jia, J. Environmental hotspot analysis of primary copper production in China and its future improvement potentials. *J. Clean. Prod.* **2022**, *370*, 133458. DOI
33. Chen, J.; Wang, Z.; Wu, Y.; et al. Environmental benefits of secondary copper from primary copper based on life cycle assessment in China. *Resour. Conserv. Recycl.* **2019**, *146*, 35-44. DOI
34. Ding, X. Research and application of product life cycle assessment and intelligent analysis in the copper smelting industry. Dissertation, Kunming University of Science and Technology, Kunming, China, 2020. (in Chinese). DOI
35. Song, X.; Yang, J.; Lu, B.; Li, B.; Zeng, G. Identification and assessment of environmental burdens of Chinese copper production from a life cycle perspective. *Front. Environ. Sci. Eng.* **2014**, *8*, 580-8. DOI
36. Kandalam, A.; Reuter, M. A.; Stelter, M.; et al. A review of top submerged lance (TSL) processing-part II: thermodynamics, slag chemistry and plant flowsheets. *Metals* **2023**, *13*, 1742. DOI
37. Wood, J.; Hoang, J.; Hughes, S. Energy efficiency of the Outotec® Ausmelt process for primary copper smelting. *JOM* **2017**, *69*, 1013-20. DOI
38. International Organization for Standardization. ISO 14044:2006, Environmental management - life cycle assessment - requirements and guidelines; ISO: Geneva, Switzerland, 2006; pp 14-15. https://www.iso.org/standard/38498.html (accessed 2026-11-11).
39. Santero, N.; Hendry, J. Harmonization of LCA methodologies for the metal and mining industry. *Int. J. Life. Cycle. Assess.* **2016**, *21*, 1543-53. DOI
40. Ekvall, T.; Finnveden, G. Allocation in ISO 14041-a critical review. *J. Clean. Prod.* **2001**, *9*, 197-208. DOI
41. Weidema, B. Avoiding co-product allocation in life-cycle assessment. *J. Ind. Ecol.* **2000**, *4*, 11-33. DOI
42. China Price Information Network. China market price monitoring reports, January–December 2025. (in Chinese). https://www.chinaprice.cn/jsdzqkgd/index.jhtml (accessed 2026-11-06).
43. Liao, K. C.; Yang, M. Operation situation and development prospect of sulfuric acid industry in China in 2025. *Eco-Ind. Sci. Phosph. Fluor. Eng.* **2026**, *41*, 1-7. (in Chinese). https://lfyf.cbpt.cnki.net/portal/journal/portal/client/paper/531c77a5e641d45c9bd62709f0ccac96 (accessed 2026-11-11).
44. Tu, J.; Luo, T. Development of "Double Flash" copper smelting technology. *Nonferrous. Met. Extr. Metall.* **2022**, *3*, 1-9. DOI
45. Kojo, I. V.; Jokilaakso, A.; Hanniala, P. Flash smelting and converting furnaces: a 50 year retrospect. *JOM* **2000**, *52*, 57-61. DOI
46. International Organization for Standardization. ISO 14067:2018, Greenhouse gases-Carbon footprint of products-requirements and guidelines for quantification; ISO: Geneva, Switzerland, 2018. https://www.iso.org/standard/71206.html (accessed 2026-11-11).
47. Intergovernmental Panel on Climate Change (IPCC). Climate change 2021: the physical science basis. Working Group I Contribution to the Sixth Assessment Report of the Intergovernmental Panel on Climate Change; Cambridge University Press, 2023. DOI
48. Database implementation & Support teams at PRé Sustainability. SimaPro Craft 10.1: what's new? 2025. https://simapro.com/wp-content/uploads/2025/03/SimaPro101WhatIsNew.pdf (accessed 2026-11-06).
49. Wernet, G.; Bauer, C.; Steubing, B.; Reinhard, J.; Moreno-Ruiz, E.; Weidema, B. The ecoinvent database version 3 (part I): overview and methodology. *Int. J. Life. Cycle. Assess.* **2016**, *21*, 1218-30. DOI
50. ecoinvent Association. ecoinvent version 3.10. 2023. https://support.ecoinvent.org/ecoinvent-version-3.10 (accessed 2026-11-06).
51. ecoinvent Association. ecoinvent Version 3.11. 2024. https://support.ecoinvent.org/ecoinvent-version-3.11 (accessed 2026-11-06).
52. Ciroth, A. ICT for environment in life cycle applications openLCA - a new open source software for life cycle assessment. *Int. J. Life. Cycle. Assess.* **2007**, *12*, 209-10. DOI
53. Cilleruelo, J. openLCA 2.1-new software release. 2024. https://www.openlca.org/openlca-2-1-new-software-release/ (accessed 2026-11-06).
54. Sphera Solutions GmbH. Life cycle assessment (LCA) software solutions. https://sphera.com/solutions/product-stewardship/life-cycle-assessment-software-and-data/ (accessed 2026-11-06).
55. Jiang, Z. L.; Xiang, S. J.; Wang, H. T.; et al. Product life cycle assessment based on online survey along supply chain. *Acta. Ecol. Sin.* **2016**, *36*, 7185-91. (in Chinese). DOI
56. World Resources Institute. Chinese Life Cycle Database (CLCD). GHG Protocol. https://ghgprotocol.org/Third-Party-Databases/CLCD (accessed 2026-11-06).
57. Norgate, T.; Haque, N. Energy and greenhouse gas impacts of mining and mineral processing operations. *J. Clean. Prod.* **2010**, *18*, 266-74. DOI
58. Northey, S.; Haque, N.; Mudd, G. Using sustainability reporting to assess the environmental footprint of copper mining. *J. Clean. Prod.* **2013**, *40*, 118-28. DOI
59. Northey, S.; Mohr, S.; Mudd, G.; Weng, Z.; Giurco, D. Modelling future copper ore grade decline based on a detailed assessment of copper resources and mining. *Resour. Conserv. Recycl.* **2014**, *83*, 190-201. DOI

60. Calvo, G.; Mudd, G.; Valero, A.; Valero, A. Decreasing ore grades in global metallic mining: a theoretical issue or a global reality? *Resources* **2016**, *5*, 36. DOI
61. Azadi, M.; Northey, S. A.; Ali, S. H.; Edraki, M. Transparency on greenhouse gas emissions from mining to enable climate change mitigation. *Nat. Geosci.* **2020**, *13*, 100-4. DOI
62. Huijbregts, M. A. J. Application of uncertainty and variability in LCA. *Int. J. Life. Cycle. Assess.* **1998**, *3*, 273-80. DOI
63. Lloyd, S. M.; Ries, R. Characterizing, propagating, and analyzing uncertainty in life-cycle assessment: a survey of quantitative approaches. *J. Ind. Ecol.* **2007**, *11*, 161-79. DOI
64. Bamber, N.; Turner, I.; Arulnathan, V.; et al. Comparing sources and analysis of uncertainty in consequential and attributional life cycle assessment: review of current practice and recommendations. *Int. J. Life. Cycle. Assess.* **2020**, *25*, 168-80. DOI
65. Weidema, B. P.; Wesnæs, M. S. Data quality management for life cycle inventories-an example of using data quality indicators. *J. Clean. Prod.* **1996**, *4*, 167-74. DOI
66. Ciroth, A.; Muller, S.; Weidema, B.; Lesage, P. Empirically based uncertainty factors for the pedigree matrix in ecoinvent. *Int. J. Life. Cycle. Assess.* **2016**, *21*, 1338-48. DOI
67. Muller, S.; Lesage, P.; Ciroth, A.; Mutel, C.; Weidema, B. P.; Samson, R. The application of the pedigree approach to the distributions foreseen in ecoinvent v3. *Int. J. Life. Cycle. Assess.* **2016**, *21*, 1327-37. DOI
68. Mo, H.; Zhang, T. Z. Data quality assessment of life cycle inventory analysis. *Res. Environ. Sci.* **2003**, *16*, 55-8. (in Chinese). DOI
69. Heijungs, R. On the number of Monte Carlo runs in comparative probabilistic LCA. *Int. J. Life. Cycle. Assess.* **2020**, *25*, 394-402. DOI
70. Henriksson, P. J.; Heijungs, R.; Dao, H. M.; Phan, L. T.; de Snoo, G. R.; Guinée, J. B. Product carbon footprints and their uncertainties in comparative decision contexts. *PLoS. One.* **2015**, *10*, e0121221. DOI
71. Ministry of Ecology and Environment of the People's Republic of China; National Bureau of Statistics; National Energy Administration. Announcement on the release of 2024 electricity carbon footprint factor data, announcement No. 19 of 2025; 2025. https://www.mee.gov.cn/xxgk2018/xxgk/xxgk01/202510/t20251024_1130734.html (accessed 2026-11-06).
72. Zhuo, Z.; Du, E.; Zhang, N.; et al. Cost increase in the electricity supply to achieve carbon neutrality in China. *Nat. Commun.* **2022**, *13*, 3172. DOI
73. Wu, Y.; Zhang, Z.; Zhu, S.; et al. Decarbonizing China's grid: provincial grid carbon footprint factors and export-embedded electricity emissions from 2020 to 2060. *Carbon. Footprints.* **2025**, *4*, 31. DOI
74. Coursol, P.; Mackey, P. J.; Kapusta, J. P. T.; Valencia, N. C. Energy consumption in copper smelting: a new Asian horse in the race. *JOM* **2015**, *67*, 1066-74. DOI

Disclaimer/Publisher's Note: All statements, opinions, and data contained in this publication are solely those of the individual author(s) and contributor(s) and do not necessarily reflect those of OAE and/or the editor(s). OAE and/or the editor(s) disclaim any responsibility for harm to persons or property resulting from the use of any ideas, methods, instructions, or products mentioned in the content.



© The Author(s) 2026. Open Access This article is licensed under a Creative Commons Attribution 4.0 International License (https://creativecommons.org/licenses/by/4.0/), which permits unrestricted use, sharing, adaptation, distribution and reproduction in any medium or format, for any purpose, even commercially, as long as you give appropriate credit to the original author(s) and the source, provide a link to the Creative Commons license, and indicate if changes were made.